Influence of lateral propagating modes on laser output characteristics in selectively oxidized vertical cavity surface-emitting lasers with double oxide layers

Yong-Zhen Huang[a]

State Key Laboratory on Integrated Optoelectronics, Institute of Semiconductors, Chinese Academy of Sciences, P.O. Box 912, Beijing 100083, People's Republic of China

The influence of lateral propagating modes on the threshold current and the spontaneous emission factor in selectively oxidized vertical cavity surface-emitting lasers (VCSELs) is investigated based on the mode behaviors of lateral propagating modes and the rate equation model. The numerical results show that the lateral propagating modes may be trapped in the aperture region for the selectively oxidized VCSEL with two oxide layers, one above and one below the active region. The output characteristics of VCSELs can be affected due to the reabsorption of the quasitrapped lateral propagating modes. A lower threshold current can be expected for a VCSEL with double oxide layers than that with a single oxide layer. The numerical results of rate equations also show that a larger spontaneous emission factor can be obtained by fitting the output–input curves for the VCSEL with double oxide layers. © *1999 American Institute of Physics.*
[S0021-8979(99)07919-0]

I. INTRODUCTION

Recently, selectively oxidation of AlAs or high Al content AlGaAs has been successfully used to form a current confined aperture and a transverse waveguiding in vertical-cavity surface-emitting lasers (VCSELs). Record low threshold currents of sub-100 μA[1–3] and power conversion efficiencies of 50%[4] were achieved from oxide confined VCSELs. The cavity mode characteristics,[5–12] the transverse mode control,[13,14] and the spontaneous emission factor β[15,16] have attracted much attention in oxide confined VCSELs. The highest value of β was obtained from selectively oxidized VCSELs with double oxide layers,[15] one above and one below the active region. Lower threshold current density and higher differential quantum efficiency were observed in the VCSELs with double oxide layers than that with a single oxide layer.[17] A VCSEL with a thicker aperture or multiple apertures might have lower loss eigenmodes, due to reduced coupling between the modes in the aperture region and otherwise planar cavity.[10]

In this article, we investigate the effect of lateral propagating modes on the laser output characteristics in selectively oxidized VCSELs. We first calculate the field distribution for the lateral propagating modes in the aperture region and the oxidized region of VCSELs with single and double oxide layers. The results show that the lateral propagating modes may be trapped in the aperture region for the VCSELs with sufficient thick double oxide layers, one above and one below the active region, due to the unmatched field distributions between the aperture and the oxidized regions. Then we investigate the output behaviors for a VCSEL with the quasitrapped lateral propagating modes by simplified rate equations. The results show that the reabsorption of the lateral propagating modes can result in a lower threshold current and a higher spontaneous emission factor.

II. THE EIGENVALUE EQUATION FOR LATERAL PROPAGATING MODES

We consider a multilayer waveguide with the z coordinate perpendicular to the layers to model the lateral propagating modes in the VCSEL as shown in Fig. 1. The lateral propagating modes, which are equivalent to the laser modes of edge-emitting lasers, propagate in the x-y plane, and the VCSEL laser mode propagates along the z direction. For a lateral propagating mode propagating along the y direction, we can write the mode wave function as

$$\phi(y,z,t) = \psi(z)\exp(i\beta y - i\omega t), \tag{1}$$

where $\beta = \beta_r + i\beta_i$ is the complex propagation constant in the y direction. The mode gain G and the mode index N for the lateral propagating modes are related to the imaginary and real parts of β by

$$G = -2\beta_i, \tag{2}$$

$$N = \beta_r/k_0, \tag{3}$$

with the free space wave number $k_0 = 2\pi/\lambda$. $\phi(y,z,t)$ represents the scalar components of electric or magnetic fields in the Cartesian coordinate system. $\psi(z)$ in the layer j, where $j = 1,2,...,m$, m is the total number of the layers of the planar waveguide, can be written as

$$\psi(z) = A_j\exp(iK_jz) + B_j\exp(-iK_jz), \tag{4}$$

where the z direction complex propagation constant in the layer j is given by

$$K_j = (k_0^2 n_j^2 - \beta^2)^{1/2}, \tag{5}$$

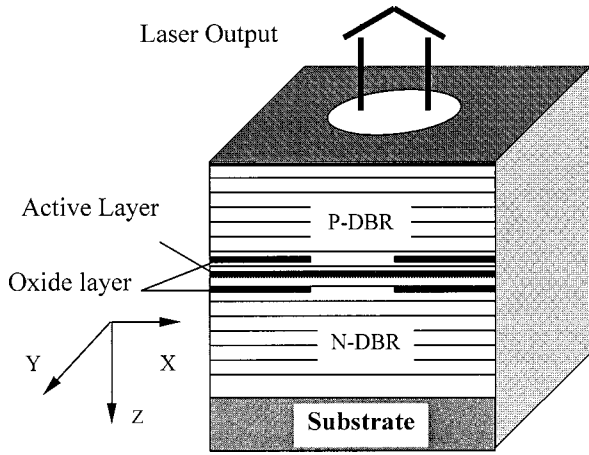[a]Electronic mail: yzhuang@red.semi.ac.cn

Laser Output

FIG. 1. The schematic diagram of a vertical-cavity surface-emitting laser with double oxide layers. The VCSEL laser mode propagates along the z direction, and the lateral propagating modes propagate in the x-y plane.

where $n_j = n_{jr} + i\kappa_j$ is the complex refractive index in the layer j, $\kappa = -g/2k_0$ is the extinction coefficient, and g is the material gain. The wave function, Eq. (4), can be considered as the sum of rays propagating along the positive and the negative z directions with complex amplitudes of A_j and B_j. In the following analysis, we consider that there are only outgoing waves in the outside regions $j=1$ and m, i.e., $A_1 = 0$ and $B_m = 0$. So the positive and the negative propagating waves are related to each other by reflectivity at the interfaces. Accounting rays reflect on the interface z_{n-1} between the layers n and $n-1$, and the interface z_n between the layers n and $n+1 (n<m)$ as waves impinge on the interfaces from the layer n, we have

$$A_n \exp(iK_n z_{n-1}) = R_{n,1} B_n \exp(-iK_n z_{n-1}), \qquad (6)$$

$$B_n \exp(-iK_n z_n) = R_{n,m} A_n \exp(iK_n z_n), \qquad (7)$$

where $R_{n,1}$ and $R_{n,m}$ are reflection coefficients including the effects of the layers $n-1$ to 1 and the layers $n+1$ to m, respectively. Multiplying Eqs. (6) and (7), we get an eigenvalue equation of

$$R_{n,1} R_{n,m} \exp(2iK_n d_n) = 1, \qquad (8)$$

where $d_n = z_n - z_{n-1}$ is the thickness of the layer n. A recursion relation for $R_{n,1}$ and $R_{n,m}$ can be derived from the boundary conditions. For TE modes, $\psi(z) = E_x(z)$ and the boundary conditions require the electric field $E_x(z)$ and its derivative $dE_x(z)/dz$ to be continuous across the boundaries. The boundary conditions in the interface z_{n-1} are

$$A_{n-1} \exp(iK_{n-1} z_{n-1}) + B_{n-1} \exp(-iK_{n-1} z_{n-1})$$
$$= A_n \exp(iK_n z_{n-1}) + B_n \exp(-iK_n z_{n-1}), \qquad (9)$$

$$K_{n-1}[A_{n-1} \exp(iK_{n-1} z_{n-1}) - B_{n-1}$$
$$\times \exp(-iK_{n-1} z_{n-1})]$$
$$= K_n[A_n \exp(iK_n z_{n-1}) - B_n \exp(-iK_n z_{n-1})]. \qquad (10)$$

By dividing Eq. (10) by Eq. (9) and using Eq. (6) to define the reflection coefficients $R_{n,1}$ and $R_{n-1,1}$, we can obtain a recursion relation as

$$R_{n,1} = \frac{R_{n,n-1} + R_{n-1,1} \exp(2iK_{n-1} d_{n-1})}{1 + R_{n,n-1} R_{n-1,1} \exp(2iK_{n-1} d_{n-1})}, \qquad (11)$$

where $d_{n-1} = z_{n-1} - z_{n-2}$ is the thickness of the layer $n-1$, and the reflection coefficient of the interface is

$$R_{n,n-1} = (K_n - K_{n-1})/(K_n + K_{n-1}). \qquad (12)$$

Similarly, a recursion relation in the same form as Eq. (11) can be obtained for $R_{n,m}$. For TM modes, $\psi(z) = H_x(z)$ and the boundary conditions require the continuity of the magnetic field $H_x(z)$ and $1/n_j^2[dH_x(z)/dx]$. The recursion relation, Eq. (11), can be used for TM modes, the only difference being that K_n and K_{n-1} in Eq. (12) should be replaced by K_n/n_n^2 and K_{n-1}/n_{n-1}^2.

III. THE MODE BEHAVIOR OF LATERAL PROPAGATING MODES

We consider a VCSEL, which consists of a 24.5-period n-$Al_{0.9}Ga_{0.1}As$/GaAs quarter-wave $(\lambda/4)$ distributed Bragg reflector (DBR), a one-wavelength-thick cavity $(\lambda$ cavity$)$ with the resonant wavelength of $\lambda=980$ nm, and a 20-period p-$Al_{0.9}Ga_{0.1}As$/GaAs $\lambda/4$ DBR. An 8-nm-thick strained InGaAs quantum well (QW) active layer is located in the center of the λ cavity, with 10 nm GaAs barriers and $Al_{0.3}Ga_{0.7}As$ confinement layers. The refractive indices of AlAs, GaAs, $Al_{0.9}Ga_{0.1}As$, $Al_{0.3}Ga_{0.7}As$, InGaAs, and AlAs–oxide are taken to be 2.88, 3.50, 2.93, 3.34, 3.6, and 1.55, respectively. The material gain of the QW region is taken to be 200 cm^{-1}. The first $\lambda/4$ $Al_{0.9}Ga_{0.1}As$ layers of the n- and p-DBR, which adjoin the λ cavity, are replaced by $\lambda/4$ AlAs–$Al_{0.9}Ga_{0.1}As$ layers, and the AlAs layers are selectively oxidized to form a current aperture. The outside layers of the VCSEL waveguide structure are air and GaAs substrate in the p-DBR and n-DBR sides, respectively. The field distributions of the lateral propagating TE modes in the aperture and the oxidized regions are calculated for the multilayer slab waveguides, with the AlAs layers and the AlAs oxide layers, respectively. The complex propagating constant β can be solved from the complex eigenvalue, Eq. (8), for the lateral propagating modes under a given wavelength, which is taken to be 980 nm in this section. With the eigenvalue β, we can obtain B_n from Eq. (6) by assuming $A_n = 1$ $(1<n<m)$, then obtain the amplitudes A_j and B_j in the other layers from the values of A_n and B_n by Eqs. (9) and (10), and finally calculate the field intensity $\psi(z)\psi^*(z)$ from Eq. (4).

The *normalized* intensity for the fundamental lateral propagating mode in the aperture region and the oxidized region are plotted as the solid and the dashed lines in Fig. 2(a), respectively, for a VCSEL with two 25 nm oxide layers. The upper lines are the refractive index distributions and the dashed line is the refractive index of the oxide layers. The horizontal axis is the distance in the z axis as shown in Fig. 1 with the zero point at the center of the active region. The corresponding optical confinement factor is 2.49% and 0.128%, respectively, for the modes in the aperture region and the oxidized region. The results show that the optical waveguide is very weak in the oxidized region, because the low refractive index of the oxide layers results in a low av-
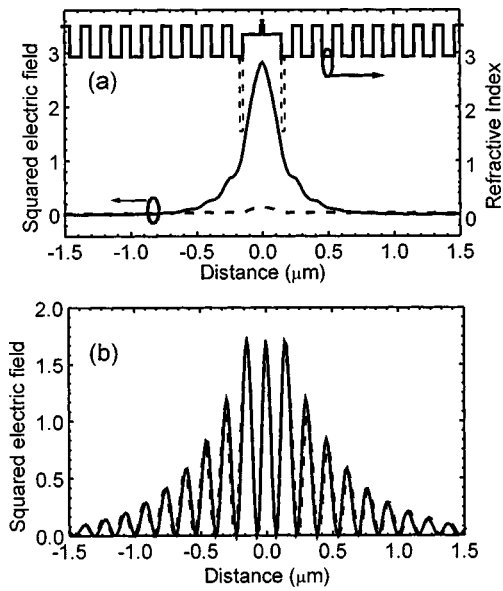
FIG. 2. The *normalized* intensity distributions for: (a) the lateral propagating fundamental mode and (b) the laser mode plotted as solid and dashed lines, respectively, in the aperture and oxidized regions for a VCSEL with two 25 nm oxide layers. The upper lines in (a) are refractive index distributions, the dashed line is the refractive index of oxide layers.
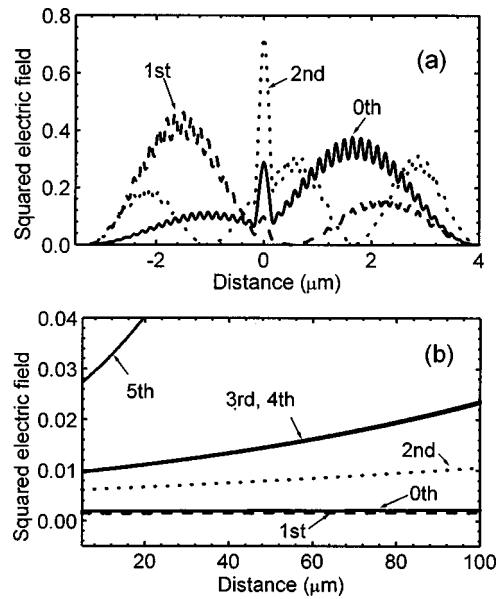
FIG. 3. The *relative* intensity distributions for the lateral propagating modes in the oxidized region of a VCSEL with two 30 nm oxide layers in: (a) the center part of the cavity and (b) the substrate.

erage index in the center. The intensity distributions for the VCSEL laser mode in the aperture and oxidized regions, i.e., the mode propagates along the z direction, are also plotted in Fig. 2(b) as the solid and dashed lines, respectively. A one-dimensional waveguide is used to calculate the intensity distribution for the VCSEL laser mode. As the distance increases from $z = 0.146$ to 0.230 μm, the intensity of the VCSEL laser mode varies from the peak to the node, and that of the lateral propagating mode only decreases from 1.20 to 0.69, based on Fig. 2. The variation of the intensity of the lateral propagating modes with the distance is much slower than that of the VCSEL laser mode. Placing the oxide layers adjoining the GaAs layers of the p-DBR and n-DBR instead of the λ cavity, i.e., at the node of the VCSEL laser mode intensity, we have the optical confinement factor of 0.47% for the lateral propagating modes in the VCSEL with two 40 nm oxide layers. And the optical confinement factor approaches zero in the VCSEL with two 41 nm oxide layers, because the field intensity is exponentially increased in the substrate. Based on the effective index model,[18] an effective index step for the VCSEL laser mode is 0.077 with the two 25 nm oxide layers as in Fig. 2, and the step is 0.022 in the case with the above two 40 nm oxide layers. So we can design a VCSEL with a weak transverse waveguiding effect for the laser mode, and still have a low average index in the center for the lateral propagating modes. The *relative* intensities for the lateral propagating modes in the oxidized region are plotted in Fig. 3 for a VCSEL with two 30 nm oxide layers. Figures 3(a) and 3(b) show the mode intensity distributions around the active region and in the substrate, respectively, the symbols 0th, 1st, 2nd, 3rd, 4th, and 5th mark the results for the fundamental, the first, the second, the third, the fourth, and the fifth order transverse modes. The number of the zero points of the intensity distribution indicates the

mode number. To express this more clearly, we only plot the intensities for the zeroth, first, and second order transverse modes in Fig. 3(a). The results show that the mode intensities increase exponentially in the substrate, so the modes are radiating modes as the oxide layers are sufficiently thick.

In Fig. 4, the mode index and the optical confinement factor versus the oxide layer thickness are plotted for the fundamental lateral propagating mode in the VCSEL with double oxide layers. The solid and dashed lines are results as the material gain of the QW is 200 and 1000 cm^{-1}, respectively. In addition to the VCSEL with single QW (SQW), we
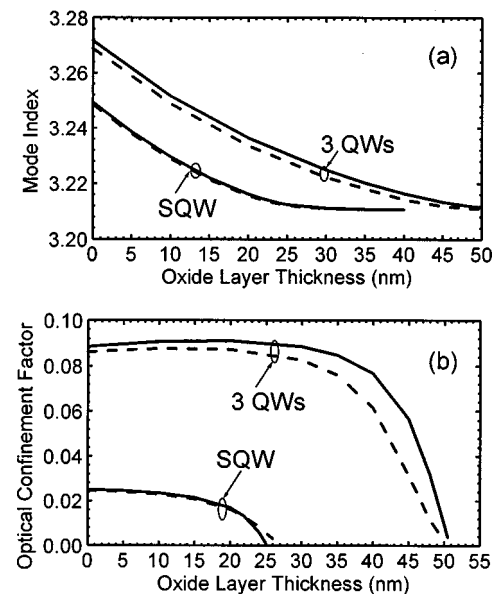
FIG. 4. The (a) mode index and (b) optical confinement factor of the lateral propagating fundamental mode in the oxidized region are plotted as functions of the thickness of the oxide layer for a VCSEL with two oxide layers. SQW and 3QWs indicate that the active region containing a single quantum well and three quantum wells, respectively.
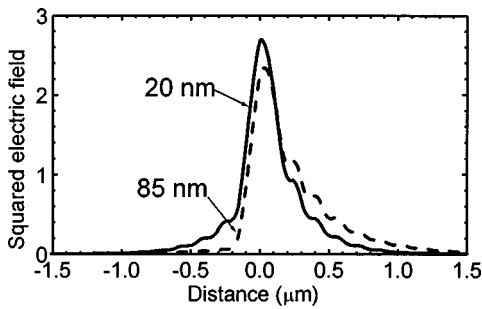
FIG. 5. The normalized intensity distribution for the fundamental lateral propagating mode in a VCSEL with a single oxide layer. The solid and dashed lines are results with a 20 and 85 nm oxide layer, respectively.

also present the mode index and the optical confinement factor for a VCSEL with three QWs (3QWs). The results show that the mode index and the optical confinement factor decrease with the increase of the oxide layer thickness. As the mode index approaches the average index of the DBR, the mode cannot be confined in the center part of the waveguide and the optical confinement factor approaches zero. The optical confinement factor approaches zero at the oxide layer thickness of 26 and 51 nm for the SQW and 3QWs cases, respectively. Because the QW has the highest refractive index, the thicker oxide layers are needed to get a divergence wave function in the case of 3QWs rather than the case of SQW. In Fig. 5, we plotted the normalized intensity for the fundamental lateral propagating mode in the oxidized region for a VCSEL with a single oxide layer, which also adjoins the λ cavity. The solid and dashed lines are results for the VCSEL with a 20 and 85 nm oxide layer, respectively. The results show that the wave function extends on the side without the oxide layer and the intensity is an asymmetric distribution. The optical confinement factor only decreases from 2.38% to 2.0% as the thickness of the oxide layer increases from 20 to 85 nm. We can expect that the coupling between the lateral propagating modes in the aperture and the oxidized regions is strong for the VCSEL with a single oxide layer.

The propagation of the lateral propagating modes through the interface between the aperture and the oxidized regions is greatly affected by the field distributions of the two regions. However, the exact solution for the mode transmitted through the interface is a very complicated problem and exceeds the scope of this article. We intend to get some heuristic conclusions from the field distributions and then discuss its effect on the VCSEL characteristics. The above numerical results show that the spatial overlap integral for the lateral propagating modes in the aperture region and the oxidized region is negligible for the VCSEL with sufficient thick double oxide layers. Based on Figs. 2(a) and 3, we can conclude that the fundamental mode in the aperture region cannot be expressed as a sum of the lateral propagating modes in the oxidized region. The lateral propagating modes will experience a large reflectivity at the interface between the aperture and the oxidized regions, because the mode reflectivity is greatly affected by the mode field distributions of the waveguides.[19] The lateral propagating mode will be a quasitrapped mode in the aperture region of the VCSEL, as

the two oxide layers, one above and one below the active region, are sufficiently thick.

IV. MODELING VCSEL OUTPUT BY RATE EQUATIONS

The quasitrapped lateral propagating modes will compete with the VCSEL laser mode based on their loss and the mode gain. The optical confinement factor is $\Gamma = 1.52\%$ and $\Gamma_t = 2.42\%$ for the laser mode and the lateral propagating modes for the VCSEL with the single 8 nm InGaAs quantum well,[20] and the mirror loss for the laser mode is $\alpha_m = 7 \ cm^{-1}$. The suppression of the lateral propagating modes requires that their loss be larger than $\Gamma_t/\Gamma = 1.59$ times the laser mode loss. Taking the material absorption $\alpha_i = 5 \ cm^{-1}$, we find that the threshold gain for the laser mode is $[\alpha_i(1-\Gamma) + \alpha_m]/\Gamma = 784 \ cm^{-1}$. The suppression of the lateral propagating modes requires that their loss α_t, which is determined by the aperture size and the mode reflectivity at the interface between the aperture and the oxidized regions, be larger than $14.1 \ cm^{-1}$. Assuming the lateral propagating modes are suppressed, we investigate their effect on the VCSEL output characteristics based on the following rate equations:

$$\frac{dS}{dt} = v_g[\Gamma g - (1-\Gamma)\alpha_i - \alpha_m]S + \Gamma\gamma\frac{N}{\tau_s}, \quad (13)$$

$$\frac{dS_l}{dt} = v_g[\Gamma_t g_l - (1-\Gamma_t)\alpha_i - \alpha_t]S_l + \Gamma_t\gamma_l\frac{N}{\tau_s}, \quad (14)$$

$$\frac{dN}{dt} = \frac{J}{eV} - \frac{N}{\tau_s} - v_g(gS + g_t s_t), \quad (15)$$

where S, $g = a(N - N_0)$, and γ (S_l, g_l, and γ_l) are the photon density, the optical gain, and the spontaneous emission factor for the laser mode (the lth mode of the lateral propagating modes), respectively. $v_g = c/n_g$ is the optical group speed, N is the carrier density, τ_s is the carrier lifetime, J is the injection current, V is the volume of the active region, and e is the electron charge. We simply use a total mode $S_t = \Sigma S_l$ to model the effect of the total lateral propagating modes under the assumption of $g_t S_t = \Sigma g_l S_l$. The spontaneous emission factor of the total mode is $\gamma_t = \Sigma\gamma_l$, which is much larger than γ. Based on the above assumptions, we get a rate equation for the total mode by summing Eq. (14) for the total lateral propagating modes:

$$\frac{dS_t}{dt} = v_g[\Gamma_t g_t - (1-\Gamma_t)\alpha_i - \alpha_t]S_t + \Gamma_t\gamma_t\frac{N}{\tau_s}. \quad (16)$$

The relative position of the laser mode wavelength and the gain peak wavelength can greatly affect the laser behaviors of a VCSEL.[21] The wavelength of the lateral propagating mode in the gain or absorption spectrum region will determine whether the mode is reabsorbed or stimulated. Most of the spontaneous emission is in the absorption spectrum region, and therefore they should have a larger transparent carrier density and a higher differential gain than the laser mode.[22] We simply take $g_t = a_t(N - N_t)$ with $a_t = 2 \times 10^{-15} \ cm^2$ and $N_t = 5 \times 10^{18} \ cm^{-3}$ to represent the optical gain for the total mode. $a = 4 \times 10^{-16} \ cm^2$ and $N_0 = 1.4 \times 10^{18} cm^{-3}$ for the laser mode, and $n_g = 4$, $\alpha_i = 5 \ cm^{-1}$, $\tau_s = 2 \times 10^{-9} \ s$
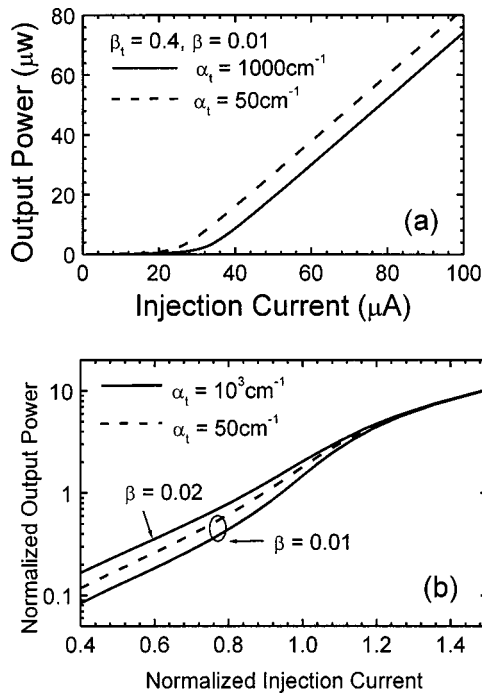
FIG. 6. (a) The modeled laser output vs the injection current for a VCSEL with trapped lateral propagating modes and $\gamma=0.01$ and $\gamma_t=0.4$. The solid and dashed lines are results at $\alpha_t=1000$ and 50 cm^{-1}, respectively. (b) The normalized laser output vs the normalized injection current for a VCSEL with $\gamma_t=0.4$. The solid lines are results at $\alpha_t=1000$ cm^{-1} and $\gamma=0.01$ and 0.02, respectively, and the dashed line is the results at $\alpha_t=50$ cm^{-1} and $\gamma=0.01$.
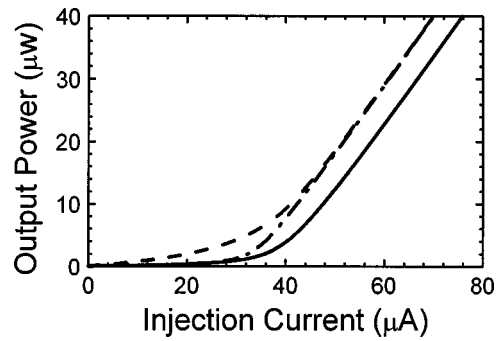

FIG. 7. The modeled laser output for a VCSEL with multitransverse modes and $\gamma=0.01$ and $\gamma_t=0.1$. The solid and dashed lines are the output power of the fundamental mode and the total output power. The dashed–dotted line is the result of single mode rate equations.

are used in the calculation. Dividing the spontaneous emission in the three directions, we can expect that the amount of the spontaneous emission in the x and the y directions, i.e., the lateral direction of the VCSEL, is about two thirds of the whole spontaneous emission. In the following simulation, we take $\gamma_t=0.4$ for the total mode of the lateral propagating modes, and calculate the laser output power as a function of the injection current for a VCSEL with the aperture area of 2×2 μm^2.

Figure 6(a) shows the laser output versus the injection current at $\gamma_t=0.4$, $\gamma=0.01$, where the solid and the dashed lines are results for the loss of the total mode α_t $=1000$ cm^{-1} and 50 cm^{-1}, respectively. Figure 6(b) shows the normalized laser output versus the normalized injection current at $\gamma_t=0.4$, $\gamma=0.01$ and 0.02, and $\alpha_t=1000$ cm^{-1} as the solid lines, and at $\gamma_t=0.4$, $\gamma=0.01$, and $\alpha_t=50$ cm^{-1} as the dashed line. The results show that a lower threshold current can be obtained for a VCSEL with a lower α_t for the lateral propagating modes. The reduction of the threshold current can be attributed to the enhancement of the carrier lifetime due to the self-absorption of spontaneously emitted photons.[23] Fitting the measured output–input curves to the results of the rate equations model,[24] we can obtain a larger spontaneous emission factor because of the reabsorption of the lateral propagating modes as shown in Fig. 6(b).

Finally, we model the laser output behaviors for a VCSEL with multitransverse modes. The rate equation (16) is used for the higher order transverse modes where the gain g_t is equal to the gain of the laser mode because the wave-

length difference between different transverse modes is usually much smaller than the width of the gain spectrum. The optical confinement factor of the higher order transverse modes is taken to be 90% of the fundamental mode because a weak optical confinement in the x-y plane for the higher order transverse modes. The mirror loss takes the same value of 7 cm^{-1} as the fundamental mode, but an extra loss of 5 cm^{-1} is assumed for the higher order transverse modes. Figure 7 shows the output power versus the injection for a VCSEL with $\gamma_t=0.1$ for the total higher order transverse modes and $\gamma=0.01$ for the laser mode. The solid line is the output power of the laser mode, i.e., the fundamental mode, and the dashed line is the total output power including the laser mode and the higher order transverse modes. The results show that two threshold currents exist from the output–input curves of the total output power and the output power of the fundamental mode. The threshold current of the fundamental mode is 39.4 μA, which is larger than 33.7 μA of the total output power. Although the increase of the spontaneous emission factor can reduce the laser threshold current,[25] the above threshold current difference is not caused by the difference between $\gamma_t=0.1$ and $\gamma=0.01$. The dashed–dotted line in Fig. 7 is the result of single mode rate equations for the laser mode, and the threshold current is 33.8 μA, which is almost the same as that of the total output power in the multitransverse modes case.

V. CONCLUSIONS

We have analyzed the effect of the lateral propagating modes on the laser output behaviors in selectively oxidized VCSELs. The results show that the lateral propagating modes may be trapped in the aperture region for a VCSEL with double oxide layers, one above and one below the active region. A simplified rate equation model shows that the reabsorption of the trapped lateral propagating modes may result in a lower threshold current and a higher apparent spontaneous emission factor for the laser mode. The influence of multitransverse modes on the output behaviors is also discussed.

ACKNOWLEDGMENTS

[1] D. L. Huffaker, D. G. Deppe, K. Humar, and T. J. Rogers, Appl. Phys. Lett. **65**, 97 (1994).

[2] Y. Hayashi, T. Mukaihara, N. Hatori, N. Ohnoki, A. Matsutani, F. Koyama, and K. Iga, Electron. Lett. **31**, 560 (1995).

[3] G. M. Yang, M. H. Macdougal, and P. D. Dapkus, Electron. Lett. **31**, 886 (1995).

[4] K. L. Lear, K. D. Choquette, R. P. Schneider, S. P. Kilcoyne, and K. M. Geib, Electron. Lett. **31**, 208 (1995).

[5] K. D. Choquette, K. L. Lear, R. P. Schneider, and K. M. Geib, Appl. Phys. Lett. **66**, 3413 (1995).

[6] G. S. Li, S. F. Lim, W. Yuen, and C. J. Chang-Hasnain, Electron. Lett. **31**, 2014 (1995).

[7] K. L. Lear, R. P. Schneider, Jr., K. D. Choquette, and S. P. Kilcoyne, IEEE Photonics Technol. Lett. **8**, 740 (1996).

[8] G. R. Hadley, Opt. Lett. **20**, 1483 (1995).

[9] L. A. Coldren, B. J. Thibeault, E. R. Hegblom, G. B. Thompson, and J. W. Scott, Appl. Phys. Lett. **68**, 313 (1996).

[10] D. G. Deppe, T.-H. Oh, and D. L. Huffaker, IEEE Photonics Technol. Lett. **9**, 713 (1997).

[11] D. G. Deppe and Q. Deng, Appl. Phys. Lett. **71**, 160 (1997).

[12] M. J. Noble, J.-H. Shin, K. D. Choquette, J. P. Loehr, J. A. Lott, and Y.-H. Lee, IEEE Photonics Technol. Lett. **10**, 4 (75)1998.

[13] M. Grabhert, R. Jäger, R. Michalzik, B. Weigl, G. Reiner, and K. J. Ebeling, IEEE Photonics Technol. Lett. **9**, 1304 (1997).

[14] Y. Z. Huang, J. Appl. Phys. **83**, 3769 (1998).

[15] D. V. Kuksenkov, H. Temkin, K. L. Lear, and H. Q. Hou, Appl. Phys. Lett. **70**, 13 (1997).

[16] J. H. Shin, Y. G. Ju, H. E. Shin, and Y. H. Lee, Appl. Phys. Lett. **70**, 2344 (1997).

[17] T.-H. Oh, D. L. Huffaker, and D. G. Deppe, IEEE Photonics Technol. Lett. **9**, 875 (1997).

[18] G. R. Hadley, Opt. Lett. **20**, 1483 (1995).

[19] T. Ikegami, IEEE J. Quantum Electron. **QE-8**, 470 (1972).

[20] Y. Z. Huang, Z. Pan, and R. H. Wu, J. Appl. Phys. **79**, 3827 (1996).

[21] T. Rössler, R. A. Indik, G. K. Harkness, J. V. Moloney, and C. Z. Ning, Phys. Rev. A **58**, 3279 (1998).

[22] C. H. Henry, in *Semiconductors and Semimetals*, 2nd ed. edited by W. T. Tsang (Academic, New York, 1985), Vol. 22.

[23] P. Asbeck, J. Appl. Phys. **48**, 820 (1977).

[24] Y. Suematsu, S. Akiba, and T. Hong, IEEE J. Quantum Electron. **13**, 596 (1977).

[25] H. Yokoyama and S. D. Bropson, J. Appl. Phys. **66**, 4801 (1989).